

Maximum-Likelihood User Localization in Active-RIS Empowered mmWave Wireless Networks

Georgios Mylonopoulos*, Luca Venturino*, Stefano Buzzi[†], Carmen D'Andrea*

*University of Cassino and Southern Latium, Cassino, Italy & CNIT, Parma, Italy

[†]University of Cassino and Southern Latium, Cassino, Italy & Politecnico di Milano, Italy & CNIT, Parma, Italy

E-mail: {georgios.mylonopoulos, l.venturino, buzzi, c.dandrea}@unicas.it

Abstract—This paper considers the user localization problem in a single-cell system operating at millimeter wave (mmWave), wherein the serving base station (BS) is aided by an active reconfigurable intelligent surface (RIS). For the considered scenario, the maximum likelihood (ML) estimator for the user position and orientation is presented, along with two sub-optimal lower-complexity estimation strategies. Numerical results are provided to show the effectiveness of the proposed solutions.

Index Terms—Active reconfigurable intelligent surfaces, mmWave, localization, position, orientation, maximum likelihood, Cramér Rao Lower Bounds.

I. INTRODUCTION

Reconfigurable Intelligent Surfaces (RISs) are attracting a huge interest both in industry and in academia for their ability to alter the propagation environment [1]. Besides improving the coverage of wireless networks, it has been recently shown that they also play a key role in user localization. Precisely, RISs are able to provide coverage to previously shadowed areas and serve as virtual anchor points [2]; moreover, they can be useful for target tracking [3], simultaneous localization and mapping (SLAM) procedures [4], and radar based localization [5] and detection [6], [7]. Controlling the RIS in such applications is not trivial. Adaptive RIS configurations have been explored, investigating the trade off between performance and training overhead [5], [8].

Traditionally, RISs consist of passive or quasi-passive elements only able to reflect the incoming EM waves. However, the multiplicative fading of the reflected signal can make the RIS useless when a strong direct link is available. To circumvent this issue, active RISs, able to also amplify the incoming wave, have been considered in both communication [9] and radar detection applications [10]. In active RISs the signal amplification gain can be controlled on a per-element basis [11] or among groups of elements [12]. Furthermore, signal processing capabilities can be added if RF chains are part of the active elements [13].

Starting from initial results in [14], we consider the problem of localizing a multi-antenna mobile station (MS) based on the signal received from a mmWave multi-antenna BS aided by an active RIS. The MS aims to find both its position in space and the orientation of its array. The corresponding ML estimator and two sub-optimal lower-complexity strategies are derived,

and their performance are compared to corresponding Cramér Rao Lower Bounds (CRLB).

Organization: This paper is organized as follows. The next section contains the description of the considered scenario and signals model. Section III contains the derivation of the maximum likelihood estimator and of its sub-optimal approximations. Numerical results are shown in Section IV, while concluding remarks are given in Section V.

Notation: Column vectors and matrices are denoted by lowercase and uppercase boldface letters, respectively. The symbols $(\cdot)^*$, $(\cdot)^T$, and $(\cdot)^H$ denote conjugate, transpose, and conjugate-transpose, respectively. \mathbf{I}_M is the $M \times M$ identity matrix. $\|\alpha\|$ is the Euclidean norm of the vector α , while $\text{vec}\{\mathbf{A}\}$ is the MN dimensional vector obtained by concatenating the columns of the $M \times N$ matrix \mathbf{A} . $\text{diag}\{\alpha\}$ is the $N \times N$ diagonal matrix with the entries of the N -dimensional vector α on the main diagonal. $\text{rank}\{\mathbf{A}\}$ and \mathbf{A}^+ are the rank and the pseudoinverse of the matrix \mathbf{A} . $\text{tr}\{\mathbf{A}\}$ and $\det\{\mathbf{A}\}$ are the trace and determinant of the square matrix \mathbf{A} . The symbol \otimes denotes the Kronecker product, while i is the imaginary unit.

II. SYSTEM MODEL

We consider an RIS-aided BS which is serving MSs located in a given region $\mathcal{M} \subset \mathbb{R}^2$, as shown in Fig. 1. The BS operates at mmWave and employs an orthogonal frequency division multiplexing (OFDM) transmission format with center carrier frequency f_o and subcarrier bandwidth W_o . We make a narrow band assumption on each subcarrier, so that $\tau_{\max} \ll 1/W_o$, where τ_{\max} is the maximum expected propagation delay, and employ a subset of K uniformly-spaced subcarriers, with W being the corresponding subcarrier spacing (an integer multiple of W_o). Also, we assume that the BS and MS employ a uniform linear array containing N_b and N_m elements with half-wavelength spacing, respectively, while the RIS is a square array containing N_r reflecting elements with half-wavelength spacing; BS, MS, and RIS are assumed to be in the each other's far-field [15]. Finally, we assume $KW \ll f_o$, so that the variation of the steering vectors and of the path loss across subcarriers can be neglected; in particular, we denote by $\alpha_b(\psi) \in \mathbb{C}^{N_b}$, $\alpha_r(\psi) \in \mathbb{C}^{N_r}$ and $\alpha_m(\psi) \in \mathbb{C}^{N_m}$ the

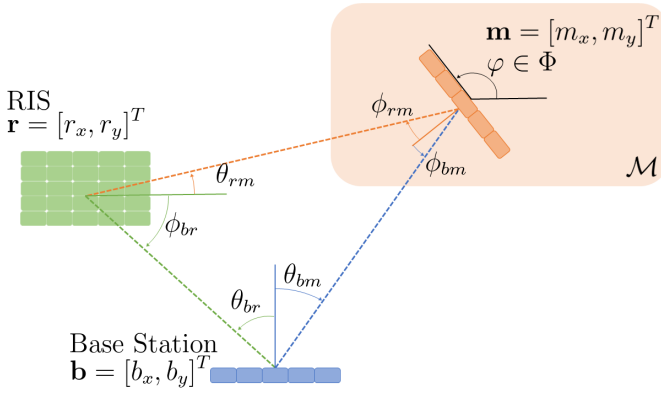


Fig. 1. Considered scenario. For simplicity, we consider a two-dimensional geometry; angles are positive when measured anti-clockwise.

steering vectors of the BS, RIS, and MS towards the direction ψ , respectively [15].

A. Transmit Signal

On each subcarrier, the BS emits Q orthogonal pilot signals over L consecutive OFDM intervals (referred to as a frame), with $Q \leq N_b$ and $L \geq Q$. The discrete-time signal emitted on the k^{th} subcarrier in the ℓ^{th} interval is

$$\mathbf{s}_k[\ell] = \sqrt{L\mathcal{P}_k} \mathbf{F}^* \mathbf{x}_k[\ell] \in \mathbb{C}^{N_b} \quad (1)$$

for $k = 1, \dots, K$ and $\ell = 1, \dots, L$, where $\mathbf{F} \in \mathbb{C}^{N_b \times Q}$ is a beamforming matrix, normalized to have $\text{tr}\{\mathbf{F}\mathbf{F}^H\} = 1$, and $\mathbf{x}_k[\ell] \in \mathbb{C}^Q$ is the vector of pilot symbols. Let $\mathbf{X}_k = [\mathbf{x}_k[1], \dots, \mathbf{x}_k[L]] \in \mathbb{C}^{Q \times L}$; we assume $\mathbf{X}_k \mathbf{X}_k^H = \mathbf{I}_Q$, so that $\mathcal{P}_k = \frac{1}{L} \sum_{\ell=1}^L \|\mathbf{s}_k[\ell]\|^2$ is the power radiated on the k^{th} subcarrier, while $\mathcal{P} = \sum_{k=1}^K \mathcal{P}_k$ is the overall radiated power.

B. Channel Model

Assuming LOS propagation with a free-space path loss model, the direct and indirect channel matrices between the BS and a MS located in the region \mathcal{M} are

$$\mathbf{H}_{k,bm} = \rho_{bm} e^{i\chi_{bm}} e^{-i2\pi\tau_{bm}Wk} \times \boldsymbol{\alpha}_m(\phi_{bm}) \boldsymbol{\alpha}_b^T(\theta_{bm}) \in \mathbb{C}^{N_m \times N_b} \quad (2a)$$

$$\mathbf{H}_{k,brm} = \rho_{brm} e^{i\chi_{brm}} e^{-i2\pi\tau_{brm}Wk} g(\theta_{rm}, \phi_{br}) \times \boldsymbol{\alpha}_m(\phi_{rm}) \boldsymbol{\alpha}_b^T(\theta_{br}) \in \mathbb{C}^{N_m \times N_b} \quad (2b)$$

respectively, where ρ is the link attenuation, χ is a phase offset, τ is the time of flight, θ and ϕ are the angles of departure and arrival, respectively, $g(\theta, \phi) = \boldsymbol{\alpha}_r^H(\theta) \text{diag}\{\boldsymbol{\omega}\} \boldsymbol{\alpha}_r(\phi)$ is the RIS array factor, and $\boldsymbol{\omega} \in \mathbb{C}^{N_r}$ contains the tunable magnitude and phase responses of the RIS elements.

C. Received Signal

The signal received by a MS located in the region \mathcal{M} on the k^{th} subcarrier in the ℓ^{th} OFDM interval is

$$\tilde{\mathbf{y}}_k[\ell] = (\mathbf{H}_{k,bm} + \mathbf{H}_{k,brm}) \mathbf{s}_k[\ell] + \tilde{\mathbf{z}}_k[\ell] + \tilde{\mathbf{v}}_k[\ell] \in \mathbb{C}^{N_m} \quad (3)$$

for $k = 1, \dots, K$ and $\ell = 1, \dots, L$, where $\tilde{\mathbf{z}}_k[\ell]$ is the noise generated by the MS receiver, while $\tilde{\mathbf{v}}_k[\ell]$ accounts for the

dynamic noise generated by the RIS. The noise terms $\tilde{\mathbf{z}}_k[\ell]$ and $\tilde{\mathbf{v}}_k[\ell]$ are mutually independent. Also, we assume that they are independent across different subcarriers and symbol intervals. The entries of $\tilde{\mathbf{z}}_k[\ell]$ are modeled as independent complex circularly-symmetric Gaussian random variables with variance σ_z^2 . Moreover, following [1], we assume that

$$\tilde{\mathbf{v}}_k[\ell] = \underbrace{\rho_{rm} e^{i\chi_{rm}} e^{-i2\pi\tau_{rm}Wk} \boldsymbol{\alpha}_r^T(\theta_{rm}) \text{diag}\{\boldsymbol{\omega}\} \tilde{\mathbf{d}}_k[\ell]}_{\tilde{\mathbf{v}}_k[\ell]} \times \boldsymbol{\alpha}_m(\phi_{rm}) \quad (4)$$

where the j^{th} entry of $\tilde{\mathbf{d}}_k[\ell]$ is the dynamic noise produced by the j^{th} element of the RIS on the k^{th} subcarrier in the ℓ^{th} symbol interval, ρ_{rm} is the link attenuation, χ_{rm} is a phase offset for the RIS-MS hop, and τ_{rm} is the time of flight. The entries of $\tilde{\mathbf{d}}_k[\ell]$ are modeled as independent complex circularly-symmetric Gaussian random variables with variance σ_d^2 so that $\tilde{\mathbf{v}}_k[\ell]$ is itself complex circularly-symmetric Gaussian with variance $\sigma_v^2 = \rho_{rm}^2 \|\boldsymbol{\omega}\|^2 \sigma_d^2$.

To proceed, we organize the signals received on the k^{th} subcarrier over L symbols intervals into a matrix. Hence, upon defining $\tilde{\mathbf{Y}}_k = [\tilde{\mathbf{y}}_k[1], \dots, \tilde{\mathbf{y}}_k[L]] \in \mathbb{C}^{N_m \times L}$, $\tilde{\mathbf{Z}}_k = [\tilde{\mathbf{z}}_k[1], \dots, \tilde{\mathbf{z}}_k[L]] \in \mathbb{C}^{N_m \times L}$, and $\tilde{\mathbf{V}}_k = [\tilde{\mathbf{v}}_k[1], \dots, \tilde{\mathbf{v}}_k[L]] \in \mathbb{C}^{N_m \times L}$, we can write

$$\tilde{\mathbf{Y}}_k = \sqrt{L\mathcal{P}_k} (\mathbf{H}_{k,bm} + \mathbf{H}_{k,brm}) \mathbf{F}^* \mathbf{X}_k + \tilde{\mathbf{Z}}_k + \tilde{\mathbf{V}}_k. \quad (5)$$

After post-multiplying $\tilde{\mathbf{Y}}_k$ by \mathbf{X}_k^H , we obtain

$$\mathbf{Y}_k = \sqrt{L\mathcal{P}_k} (\mathbf{H}_{k,bm} + \mathbf{H}_{k,brm}) \mathbf{F}^* + \mathbf{Z}_k + \mathbf{V}_k \in \mathbb{C}^{N_m \times Q} \quad (6)$$

where $\mathbf{Z}_k = \tilde{\mathbf{Z}}_k \mathbf{X}_k^H$ and $\mathbf{V}_k = \tilde{\mathbf{V}}_k \mathbf{X}_k^H$. Finally, we organize the signals in (6) across all subcarriers into a vector. Upon defining $\mathbf{y}_k = \text{vec}\{\mathbf{Y}_k\} \in \mathbb{C}^{N_m Q}$ and $\mathbf{y} = \text{vec}\{\mathbf{y}_1 \dots \mathbf{y}_K\} \in \mathbb{C}^{KQ N_m}$, we have

$$\mathbf{y} = e^{i\chi_{bm}} \mathbf{s}_{bm}(\mathbf{m}, \varphi) + e^{i\chi_{brm}} \mathbf{s}_{brm}(\mathbf{m}, \varphi) + \mathbf{z} + \mathbf{v}. \quad (7)$$

In the above equation, the vectors

$$\mathbf{s}_{bm}(\mathbf{m}, \varphi) = \rho_{bm} \mathbf{t}(\tau_{bm}) \otimes \mathbf{F}^H \mathbf{a}_b(\theta_{bm}) \otimes \mathbf{a}_m(\phi_{bm}) \quad (8a)$$

$$\mathbf{s}_{brm}(\mathbf{m}, \varphi) = \rho_{brm} g(\theta_{rm}, \phi_{br}) \times \mathbf{t}(\tau_{brm}) \otimes \mathbf{F}^H \mathbf{a}_b(\theta_{br}) \otimes \mathbf{a}_m(\phi_{rm}) \quad (8b)$$

are the signatures of signals received by the MS along the direct and the indirect path, respectively, which are uniquely specified by its position \mathbf{m} and orientation φ , while

$$\mathbf{t}(\tau) = [\sqrt{L\mathcal{P}_1} e^{-i2\pi\tau W} \dots \sqrt{L\mathcal{P}_K} e^{-i2\pi\tau WK}]^T \in \mathbb{C}^K. \quad (9)$$

Finally, the noise terms \mathbf{z} and \mathbf{v} are defined similarly to \mathbf{y} ; in particular, they are independent complex circularly-symmetric Gaussian vectors with covariance matrices $\sigma_z^2 \mathbf{I}_{KQ N_m}$ and $\mathbf{I}_{KQ} \otimes \sigma_v^2 \mathbf{a}_m(\phi_{rm}) \mathbf{a}_m^H(\phi_{rm})$, respectively.

III. MAXIMUM LIKELIHOOD ESTIMATION

Assuming that $x_{bm} = e^{i\chi_{bm}}$ and $x_{brm} = e^{i\chi_{brm}}$ are deterministic unknown quantities, the likelihood function of the received signal \mathbf{y} can be written as

$$f(\mathbf{y}; \mathbf{x}, \mathbf{m}, \varphi) = \frac{1}{\pi^{KQ} N_m \det\{\mathbf{C}(\mathbf{m}, \varphi)\}} \exp\left\{-\left\|\mathbf{C}^{-1/2}(\mathbf{m}, \varphi)(\mathbf{y} - \mathbf{S}(\mathbf{m}, \varphi)\mathbf{x})\right\|^2\right\} \quad (10)$$

where $\mathbf{S}(\mathbf{m}, \varphi) = [\mathbf{s}_{bm}(\mathbf{m}, \varphi), \mathbf{s}_{brm}(\mathbf{m}, \varphi)]$, $\mathbf{x} = [x_{bm}, x_{brm}]^T$, and

$$\mathbf{C}(\mathbf{m}, \varphi) = \mathbf{I}_{KQ} \otimes \underbrace{(\sigma_z^2 \mathbf{I}_{N_m} + \sigma_v^2 \mathbf{a}_m(\phi_{rm}) \mathbf{a}_m^H(\phi_{rm}))}_{\mathbf{C}_m(\mathbf{m}, \varphi)}. \quad (11)$$

Upon exploiting the structure of the noise covariance matrix, it is easily verified that

$$\det\{\mathbf{C}(\mathbf{m}, \varphi)\} = \left((N_m \sigma_v^2 + \sigma_z^2) \sigma_z^{2(N_m-1)}\right)^{KQ} \quad (12a)$$

$$\mathbf{C}^{-1}(\mathbf{m}, \varphi) = \mathbf{I}_{KQ} \otimes \frac{1}{\sigma_z^2} \left(\mathbf{I}_{N_m} - \frac{\sigma_v^2 \mathbf{a}_m(\phi_{rm}) \mathbf{a}_m^H(\phi_{rm})}{\sigma_z^2 + N_m \sigma_v^2} \right). \quad (12b)$$

To proceed, we first compute the ML estimate of \mathbf{x} for a given \mathbf{m} and φ , i.e.,

$$\begin{aligned} \hat{\mathbf{x}}(\mathbf{m}, \varphi) &= \arg \max_{\mathbf{x} \in \mathbb{C}^2: |x_{bm}|=|x_{brm}|=1} f(\mathbf{y}; \mathbf{x}, \mathbf{m}, \varphi) \\ &= \arg \min_{\mathbf{x} \in \mathbb{C}^2: |x_{bm}|=|x_{brm}|=1} \Re \left\{ x_{bm}^* x_{brm} \kappa(\mathbf{m}, \varphi) \right. \\ &\quad \left. - x_{bm}^* \kappa_{bm}(\mathbf{m}, \varphi) - x_{brm}^* \kappa_{brm}(\mathbf{m}, \varphi) \right\}. \quad (13) \end{aligned}$$

where we have defined

$$\kappa(\mathbf{m}, \varphi) = \mathbf{s}_{bm}^H(\mathbf{m}, \varphi) \mathbf{C}^{-1}(\mathbf{m}, \varphi) \mathbf{s}_{brm}(\mathbf{m}, \varphi) \quad (14a)$$

$$\kappa_{bm}(\mathbf{m}, \varphi) = \mathbf{s}_{bm}^H(\mathbf{m}, \varphi) \mathbf{C}^{-1}(\mathbf{m}, \varphi) \mathbf{y} \quad (14b)$$

$$\kappa_{brm}(\mathbf{m}, \varphi) = \mathbf{s}_{brm}^H(\mathbf{m}, \varphi) \mathbf{C}^{-1}(\mathbf{m}, \varphi) \mathbf{y}. \quad (14c)$$

Finally, the ML estimate of the MS position and orientation is obtained as

$$\begin{aligned} [\hat{\mathbf{m}}, \hat{\varphi}] &= \arg \max_{\substack{\mathbf{m} \in \mathcal{M} \\ \varphi \in \Phi}} f(\mathbf{y}; \hat{\mathbf{x}}(\mathbf{m}, \varphi), \mathbf{m}, \varphi) \\ &= \arg \min_{\substack{\mathbf{m} \in \mathcal{M} \\ \varphi \in \Phi}} \left\| \mathbf{C}^{-1/2}(\mathbf{m}, \varphi) (\mathbf{y} - \mathbf{S}(\mathbf{m}, \varphi) \hat{\mathbf{x}}(\mathbf{m}, \varphi)) \right\|^2 \quad (15) \end{aligned}$$

where the search interval $\Phi \subseteq [0, 2\pi]$ is tied to the prior uncertainty on the MS orientation.

The following remarks are now in order. The implementation of (15) requires a joint search among \mathbf{m} , φ , and \mathbf{x} , which may entail a prohibitive computational complexity. Also, the knowledge of both the beamforming matrix \mathbf{F} and the RIS response $\boldsymbol{\omega}$ is required at the MS, which may entail an additional signaling overhead. To overcome these limitations, we propose next two sub-optimal estimators.

A. Sub-optimal estimator

We remove here the unimodular constraint on the entries of \mathbf{x} in (13). The corresponding relaxed problem is convex and its minimum value is attained when

$$\tilde{\mathbf{x}}(\mathbf{m}, \varphi) = \left(\mathbf{C}^{-1/2}(\mathbf{m}, \varphi) \mathbf{S}(\mathbf{m}, \varphi) \right)^+ \mathbf{C}^{-1/2}(\mathbf{m}, \varphi) \mathbf{y}. \quad (16)$$

At this point, we propose to plug the above estimate in (15) upon normalizing its entries to have unit-modulus.

B. Sub-optimal estimator with limited information

Let $\mathbf{y}_k^{(q)}$ be the q^{th} column of the matrix \mathbf{Y}_k in (6) and let $\mathbf{y}^{(q)} = \text{vec} \left\{ \left(\mathbf{y}_1^{(q)} \dots \mathbf{y}_K^{(q)} \right) \right\} \in \mathbb{C}^{KN_m}$; also, let

$$p_{bm}^{(q)} = \rho_{bm} e^{i\chi_{bm}} \left[\mathbf{a}_b^T(\theta_{bm}) \mathbf{F}^* \right]_q \quad (17a)$$

$$p_{brm}^{(q)} = g(\theta_{rm}, \phi_{br}) \rho_{brm} e^{i\chi_{brm}} \left[\mathbf{a}_b^T(\theta_{rm}) \mathbf{F}^* \right]_q. \quad (17b)$$

Then, we have

$$\mathbf{y}^{(q)} = \bar{\mathbf{S}}(\mathbf{m}, \varphi) \mathbf{p}^{(q)} + \mathbf{z}^{(q)} + \mathbf{v}^{(q)} \quad (18)$$

where $\bar{\mathbf{S}}(\mathbf{m}, \varphi) = [\mathbf{t}(\tau_{bm}) \otimes \mathbf{a}_m(\phi_{bm}), \mathbf{t}(\tau_{brm}) \otimes \mathbf{a}_m(\phi_{rm})]$ and $\mathbf{p}^{(q)} = [p_{bm}^{(q)}, p_{brm}^{(q)}]^T$, while the noise vectors $\mathbf{z}^{(q)}$ and $\mathbf{v}^{(q)}$ are defined similarly to $\mathbf{y}^{(q)}$.

Assuming at the design stage that $\mathbf{p}^{(q)}$ is an unknown deterministic parameter, then its ML estimate can be found in closed form and is given by

$$\begin{aligned} \check{\mathbf{p}}^{(q)}(\mathbf{m}, \varphi) &= \arg \max_{\mathbf{p}^{(q)} \in \mathbb{C}^2} \bar{f}(\mathbf{y}^{(q)}; \mathbf{p}^{(q)}, \mathbf{m}, \varphi) \\ &= \left(\bar{\mathbf{C}}^{-1/2}(\mathbf{m}, \varphi) \bar{\mathbf{S}}(\mathbf{m}, \varphi) \right)^+ \bar{\mathbf{C}}^{-1/2}(\mathbf{m}, \varphi) \mathbf{y}^{(q)} \quad (19) \end{aligned}$$

where

$$\begin{aligned} \bar{f}(\mathbf{y}^{(q)}; \mathbf{p}^{(q)}, \mathbf{m}, \varphi) &= \frac{1}{\pi^{KN_m} \det\{\bar{\mathbf{C}}^{-1/2}(\mathbf{m}, \varphi)\}} \\ &\times \exp \left\{ - \left\| \bar{\mathbf{C}}^{-1/2}(\mathbf{m}, \varphi) (\mathbf{y}^{(q)} - \bar{\mathbf{S}}(\mathbf{m}, \varphi) \mathbf{p}^{(q)}) \right\|^2 \right\} \quad (20) \end{aligned}$$

is the likelihood function of $\mathbf{y}^{(q)}$ and $\bar{\mathbf{C}}^{-1/2}(\mathbf{m}, \varphi) = \mathbf{I}_K \otimes \mathbf{C}_m^{-1/2}(\mathbf{m}, \varphi)$. A sub-optimal estimate of the MS position and orientation can now be obtained as follows

$$\begin{aligned} [\check{\mathbf{m}}, \check{\varphi}] &= \arg \max_{\substack{\mathbf{m} \in \mathcal{M} \\ \varphi \in \Phi}} \prod_{q=1}^Q \bar{f}(\mathbf{y}^{(q)}; \check{\mathbf{p}}^{(q)}(\mathbf{m}, \varphi), \mathbf{m}, \varphi) \\ &= \arg \min_{\substack{\mathbf{m} \in \mathcal{M} \\ \varphi \in \Phi}} \sum_{q=1}^Q \left\| \left(\mathbf{I}_{KN_m} - \bar{\mathbf{\Pi}}(\mathbf{m}, \varphi) \right) \bar{\mathbf{C}}^{-1/2}(\mathbf{m}, \varphi) \mathbf{y}^{(q)} \right\|^2 \quad (21) \end{aligned}$$

where $\bar{\mathbf{\Pi}}(\mathbf{m}, \varphi)$ is the orthogonal projector onto the column span of $\bar{\mathbf{C}}^{-1/2}(\mathbf{m}, \varphi) \bar{\mathbf{S}}(\mathbf{m}, \varphi)$. This estimator does not require knowledge of \mathbf{F} and $\boldsymbol{\omega}$ and entails the computation of lower dimensional matrices (as compared to the former two).

IV. PERFORMANCE ANALYSIS

A. CRLB computation

As a benchmark, we include in our analysis the CRLBs on the position and the orientation estimations. To this end, notice that the Fisher Information Matrix (FIM), say $\bar{\mathbf{J}}$, of the unknown parameters $\boldsymbol{\eta} = [\tau_{bm}, \theta_{bm}, \phi_{bm}, \rho_{bm}, \tau_{rm}, \theta_{rm}, \phi_{rm}, \rho_{rm}, \chi_{bm}, \chi_{brm}]^T$ is

$$[\bar{\mathbf{J}}(\mathbf{m}, \varphi)]_{i,j} = \frac{\partial \boldsymbol{\mu}(\mathbf{m}, \varphi)^H}{\partial \eta_i} \mathbf{C}^{-1}(\mathbf{m}, \varphi) \frac{\partial \boldsymbol{\mu}(\mathbf{m}, \varphi)}{\partial \eta_j} + \frac{1}{2} \text{tr} \left\{ \mathbf{C}^{-1}(\mathbf{m}, \varphi) \frac{\partial \mathbf{C}(\mathbf{m}, \varphi)}{\partial \eta_i} \mathbf{C}^{-1}(\mathbf{m}, \varphi) \frac{\partial \mathbf{C}(\mathbf{m}, \varphi)}{\partial \eta_j} \right\}. \quad (22)$$

where $\boldsymbol{\mu}(\mathbf{m}, \varphi)$ is the noise-free signal, i.e.,

$$\boldsymbol{\mu}(\mathbf{m}, \varphi) = e^{i\chi_{bm}} \mathbf{s}_{bm}(\mathbf{m}, \varphi) + e^{i\chi_{brm}} \mathbf{s}_{brm}(\mathbf{m}, \varphi). \quad (23)$$

Upon defining the transformation $\mathbf{T} = \partial \boldsymbol{\eta} / \partial \boldsymbol{\zeta}$, where $\boldsymbol{\zeta} = [m_x, m_y, \varphi]^T$, the FIM of $\boldsymbol{\zeta}$ is $\mathbf{J}(\mathbf{m}, \varphi) = \mathbf{T} \bar{\mathbf{J}}(\mathbf{m}, \varphi) \mathbf{T}^T$. Accordingly, the positioning error bound (PEB) and the orientation error bound (OEB) are given by

$$\text{PEB}(\mathbf{m}, \varphi) = \sqrt{\text{tr} \{ [\mathbf{J}(\mathbf{m}, \varphi)^{-1}]_{1:2,1:2} \}} \quad [\text{m}] \quad (24a)$$

$$\text{OEB}(\mathbf{m}, \varphi) = \sqrt{[\mathbf{J}(\mathbf{m}, \varphi)^{-1}]_{3,3}} \quad [\text{rad}]. \quad (24b)$$

B. Simulation setup

We assume a carrier frequency of $f_o = 60$ GHz and select $K = 16$ subcarriers spaced of $W = 6$ MHz each. We consider the system geometry in Fig. 1, with $\mathbf{b} = (0, 0)$ m, $\mathbf{r} = (50 \cos(-\pi/6), 50 \sin(-\pi/6))$ m, $\mathcal{M} = [22.5, 41] \times [27.5, 46]$ m², and $\Phi = [\pi/2, \pi]$. Unless otherwise specified, we set $N_b = 64$, $N_r = 32^2$, and $N_m = 4$. The RIS response is designed to steer the main beam towards the center of the inspected region, while the amplification gain of each element is 40 dB. Finally, we assume a noise power spectral density of -174 dBm/Hz, with a 5 dB noise figure of the receiver.

C. Numerical Results

We provide here some numerical examples to assess the performance of the proposed estimators. The shown results are an average over random realizations of the MS (position and orientation) within the considered region.

Figs. 2 and 3 show the performance for the proposed estimators versus the SNR, in terms of root mean square error (RMSE). The figures also include the system's CRLBs for the cases of an active and a passive RIS and when a RIS is not utilized. In the latter RIS-free scenario, all the available power at the BS is directed at \mathcal{M} ($Q = 1$). It is shown that the ML estimator performance is almost identical to the CRLBs. The positioning accuracy of strategies III.A and III.B experience a 5 dB and 10 dB performance delay, respectively, compared to the ML estimator. For the orientation estimation the delay is close to 2 dB. Interestingly, sub-optimal strategy III.A outperforms the CRLBs of the passive RIS system, while III.B outperforms the OEB of the passive RIS system.

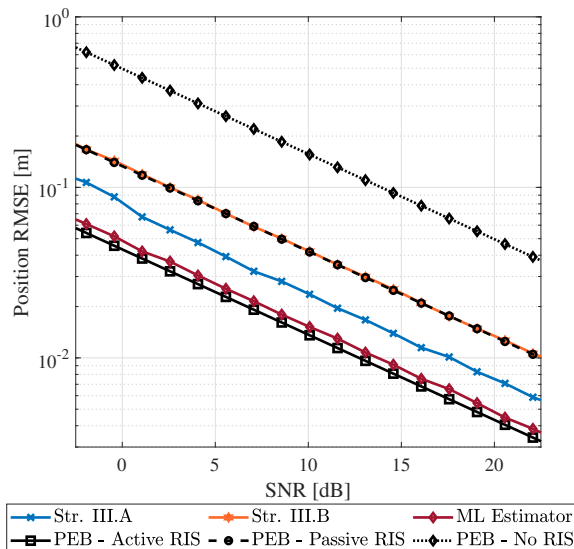


Fig. 2. Position RMSE for the proposed estimators & PEB for different SNR values.

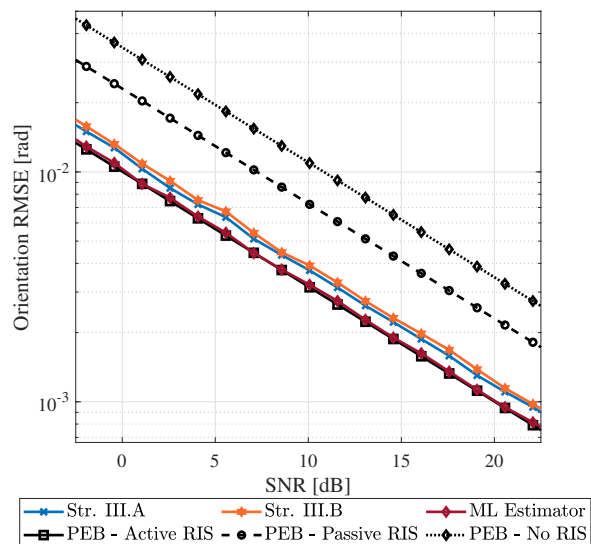


Fig. 3. Orientation RMSE for the proposed estimators & OEB for different SNR values.

Next, Figs. 4 and 5 assess the effects of the RIS size and number of antennas at the MS. Precisely, the figures show the CRLBs for the MS location and orientation, respectively, versus the number of antennas at the MS, for several RIS sizes. Since the RIS gain per element is constant (40 dB), the consumed power grows linearly with the number of RIS elements. Results show that the performance improves as the RIS size and the number of antenna elements increases. It needs to be noted that increasing the number of receive antennas reduces the OEBs more drastically.

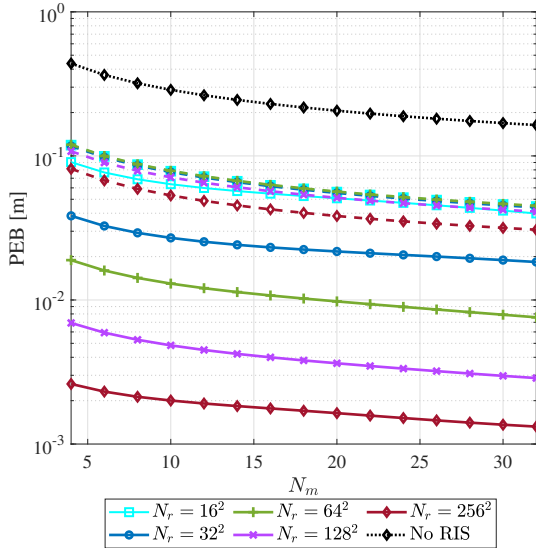


Fig. 4. PEB for different number of receive antennas and RIS sizes. The solid lines represent an active RIS and the dashed lines a passive one.

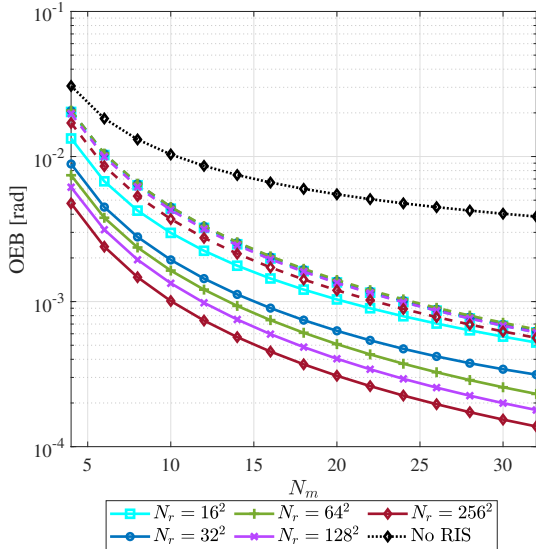


Fig. 5. OEB for different number of receive antennas and RIS sizes. The solid lines represent an active RIS and the dashed lines a passive one.

V. CONCLUSIONS

This paper has been focused on the derivation of estimation strategies for an MS location and antenna array orientation in a single-cell wireless network aided by an active RIS and operating under LoS conditions at mmWave carrier frequencies. The ML estimator has been first derived, under the assumption that the RIS was set to direct the incoming path towards the area where the mobile station was supposed to be. Then, in order to reduce complexity, two sub-optimal strategies have been also proposed. The performance analysis

has revealed that the proposed estimation algorithms work well and approach the CRLB for large SNR values. Moreover, it has been shown that the presence of a RIS improves the localization performance with respect to the case of no RIS, as well as that the increase of the RIS size and of the number of antennas at the MS have a beneficial effect on the performance. Current work in this area is devoted to the design of adaptive RIS configuration strategies to enable localization in multiple neighboring regions, as well as to the investigation of additional sub-optimal estimators capable of better approaching the performance of the ML strategy.

VI. ACKNOWLEDGEMENTS

This work was supported by the EU Horizon 2020 MSCA-ITN-METAWIRELESS Project, Grant Agreement 956256.

REFERENCES

- [1] E. Basar, M. Di Renzo, J. De Rosny, M. Debbah, M.-S. Alouini, and R. Zhang, "Wireless communications through reconfigurable intelligent surfaces," *IEEE Access*, vol. 7, pp. 116753–116773, Aug. 2019.
- [2] D. Dardari, N. Decarli, A. Guerra, and F. Guidi, "Los/nlos near-field localization with a large reconfigurable intelligent surface," *IEEE Transactions on Wireless Communications*, 2021.
- [3] D. Dardari, N. Decarli, A. Guerra, and F. Guidi, "Localization in nlos conditions using large reconfigurable intelligent surfaces," in *2021 IEEE 22nd International Workshop on Signal Processing Advances in Wireless Communications (SPAWC)*, pp. 551–555, IEEE, 2021.
- [4] H. Wymeersch, J. He, B. Denis, A. Clemente, and M. Juntti, "Radio localization and mapping with reconfigurable intelligent surfaces: Challenges, opportunities, and research directions," *IEEE Vehicular Technology Magazine*, vol. 15, pp. 52–61, Dec. 2020.
- [5] E. Čišija, A. M. Ahmed, A. Sezgin, and H. Wymeersch, "RIS-aided mmWave MIMO radar system for adaptive multi-target localization," in *2021 IEEE Statistical Signal Processing Workshop (SSP)*, pp. 196–200, IEEE, July 2021.
- [6] S. Buzzi, E. Grossi, M. Lops, and L. Venturino, "Radar target detection aided by reconfigurable intelligent surfaces," *IEEE Signal Processing Letters*, vol. 28, pp. 1315–1319, 2021.
- [7] S. Buzzi, E. Grossi, M. Lops, and L. Venturino, "Foundations of mimo radar detection aided by reconfigurable intelligent surfaces," *IEEE Transactions on Signal Processing*, vol. 70, pp. 1749–1763, 2022.
- [8] J. He, H. Wymeersch, T. Sanguanpuak, O. Silven, and M. Juntti, "Adaptive beamforming design for mmWave RIS-aided joint localization and communication," in *2020 IEEE Wireless Communications and Networking Conference Workshops (WCNCW)*, pp. 1–6, Apr. 2020.
- [9] Z. Zhang, L. Dai, X. Chen, C. Liu, F. Yang, R. Schober, and H. V. Poor, "Active RIS vs. passive RIS: Which will prevail in 6G?," *Arxiv preprint Online available at arXiv:2103.15154v*, Mar. 2021.
- [10] M. Rihan, E. Grossi, L. Venturino, and S. Buzzi, "Spatial diversity in radar detection via active reconfigurable intelligent surfaces," *IEEE Signal Processing Letters*, vol. 29, pp. 1242–1246, 2022.
- [11] S. Taravati and G. V. Eleftheriades, "Full-duplex reflective beamsteering metasurface featuring magnetless nonreciprocal amplification," *Nature Communications*, vol. 12, no. 1, pp. 1–11, 2021.
- [12] G. C. Alexandropoulos and E. Vlachos, "A hardware architecture for reconfigurable intelligent surfaces with minimal active elements for explicit channel estimation," in *ICASSP 2020 - 2020 IEEE International Conference on Acoustics, Speech and Signal Processing (ICASSP)*, pp. 9175–9179, May 2020.
- [13] G. C. Alexandropoulos, I. Vinieratou, and H. Wymeersch, "Localization via multiple reconfigurable intelligent surfaces equipped with single receive RF chains," *IEEE Wireless Communications Letters*, vol. 11, pp. 1072–1076, May 2022.
- [14] G. Mylonopoulos, C. D'Andrea, and S. Buzzi, "Active reconfigurable intelligent surfaces for user localization in mmwave mimo systems," in *2022 IEEE 23rd International Workshop on Signal Processing Advances in Wireless Communication (SPAWC)*, pp. 1–5, IEEE, 2022.
- [15] W. L. Stutzman and G. A. Thiele, *Antenna Theory and Design*. New York, NY, USA: John Wiley & Sons, 3 ed., 1998.